Higher entropy conservation and numerical stability of compressible turbulence simulations

Albert E. Honein *, Parviz Moin

Center for Turbulence Research, Stanford University, Building 500, Stanford, CA 94305, USA

Abstract

We present a numerical formulation for the treatment of nonlinear instabilities in shock-free compressible turbulence simulations. The formulation is high order and contains no artificial dissipation. Numerical stability is enhanced through semi-discrete satisfaction of global conservation properties stemming from the second law of thermodynamics and the entropy equation. The numerical implementation is achieved using a conservative skew-symmetric splitting of the nonlinear terms. The robustness of the method is demonstrated by performing unresolved numerical simulations and large eddy simulations of compressible isotropic turbulence at a very high Reynolds number. Results show the scheme is capable of capturing the statistical equilibrium of low Mach number compressible turbulent fluctuations at infinite Reynolds number. Comparisons with the entropy splitting technique [J. Comput. Phys. 162 (2000) 33; J. Comput. Phys. 178 (2002) 307], staggered method [J. Comput. Phys. 191(2) (2003) 392], and skew-symmetric like schemes [J. Comput. Phys. 161 (2000) 114] confirm the superiority of the current approach. We also discuss a flaw in the skew-symmetric splitting implemented in the literature. Very good results are obtained based on the proper splitting.
© 2004 Elsevier Inc. All rights reserved.

Keywords: Nonlinear numerical stability; Conservation properties; Skew-symmetric form; Compressible turbulence simulations; High order central schemes

1. Introduction

Nonlinear instabilities have been a major hurdle in turbulence simulations [5,6]. They become more pronounced when high order non-dissipative methods are used in under-resolved simulations, where aliasing errors significantly increase. This is the typical situation in large eddy simulations (LES), where high order schemes are preferred in order to keep truncation errors smaller than subgrid scale terms [7]. In incompressible simulations, instabilities were successfully suppressed without artificial dissipation by

---

ensuring simultaneous discrete or semi-discrete conservation of mass, momentum, and kinetic energy in the limit of zero viscosity [8]. This can be accomplished in spectral methods through de-aliasing of the nonlinear products [9]. Alternatively, the convective terms in the momentum equation can be discretized with the skew-symmetric or rotational forms without de-aliasing. This procedure is not always accurate, as reported for the rotational form by Zang [10] and Horiuti [11]. For finite difference schemes, these forms can also be applied for conservation [12], but the preferred alternative has been the use of staggered grid [13], which also avoids the problem of even-odd grid decoupling of pressure [14]. A comparative study of all these methods can be found in [15].

Generalization of the aforementioned methods to compressible flows has not been as successful since discrete conservation of mass, momentum, and total energy do not guarantee numerical stability [16]. Robust simulations have been limited to moderate Reynolds numbers. Feiereisen et al. [17] showed that writing the convective terms in the momentum equation in skew-symmetric form ensures that these terms do not artificially contribute to the global kinetic energy, as dictated by the continuous equations. The skew-symmetric splitting yielded relatively stable simulations for LES [18,19] and DNS [20,21] of compressible isotropic turbulence with central high order compact schemes. For pseudo-spectral collocation methods, Blaisdell et al. [22] showed that the skew-symmetric form reduces aliasing errors compared to the so-called conservative and non-conservative forms. Satisfactory results were obtained by applying this form to the convective terms in both momentum and energy equations. Ducros et al. [4] followed the same steps in a finite difference/volume context. In a different study, Lee [23] reported instabilities if the total energy equation is employed instead of the internal energy equation. More recently, Nagarajan et al. [3] applied the staggered scheme in [13] to the full compressible equations and obtained better numerical stability properties compared to the collocated version.

Another approach falls within the context of mathematical entropy conservation instead of energy conservation or aliasing error minimization. Harten [24] showed how the Euler equations of gas dynamics can be written in a symmetric form cast in a new set of variables called the entropy variables. The symmetric form has the benefit of conserving strong as well as weak solutions of the original equations. Tadmor [25] extended the symmetric form to a skew self-adjoint form, when the entropy function is homogeneous in the original variables. The skew self-adjoint form forces the new set of equations to satisfy the global entropy conservation of the original Euler equations when considering reversible closed systems. This result has been independently derived by Olsson and Oliger [26] using non-homogeneous entropy functions. The skew self-adjoint form has been termed canonical splitting in [26]. Gerritsen [27] and Gerritsen and Olsson [28] applied the canonical splitting to two-dimensional compressible Euler equations with high order central-differencing. Yee et al. [1] showed that this splitting reduces nonlinear instabilities for smooth flows as well as turbulent flows involving shocks. Sandham et al. [2] obtained accurate results for compressible turbulent channel flow at low Reynolds and Mach numbers. The canonical splitting was referred to as entropy splitting in [1]. The non-uniqueness of the entropy function [24] makes this approach a function of a free parameter, β. As reported by Sandham et al. [2], results can become unstable depending on the values of β. Also, the optimum β for stability is a function of the problem being studied, which makes entropy splitting unattractive. Adaptive selection of β at each grid point as a function of the local Reynolds and Mach numbers is currently being investigated [2].

All the methods mentioned above become unstable at increasing Reynolds numbers, even at small turbulence Mach number and in the absence of shocks. We provide below a numerical formulation of the Navier–Stokes equations that possesses excellent nonlinear numerical stability properties at high Reynolds numbers. We first discuss the numerical implementation of the formulation and then show through numerical experiments and comparisons with the work cited above how numerical stability is enhanced.

2. Numerical formulation

2.1. Mathematical equations

Consider the Navier–Stokes equations:

$$\frac{\partial \rho}{\partial t} + \frac{\partial \rho u_i}{\partial x_i} = 0,$$ (1)

$$\frac{\partial \rho u_i}{\partial t} + \frac{\partial \rho u_i u_j}{\partial x_j} + \frac{\partial p}{\partial x_i} = \frac{\partial \tau_{ij}}{\partial x_j},$$ (2)

$$\frac{\partial E}{\partial t} + \frac{\partial E u_j}{\partial x_j} + \frac{\partial p u_j}{\partial x_j} = \frac{\partial \tau_{ij} u_i}{\partial x_j} + \frac{\partial}{\partial x_j}\left(\kappa \frac{\partial T}{\partial x_j}\right),$$ (3)

where

$$\tau_{ij} = \mu\left(\frac{\partial u_i}{\partial x_j} + \frac{\partial u_j}{\partial x_i}\right) - \frac{2}{3}\mu\frac{\partial u_k}{\partial x_k}\delta_{ij} \quad \text{and} \quad E = \rho\frac{u_i u_i}{2} + \rho C_v T.$$ (4)

In these equations, ρ is the density, u_i is the velocity field, p is the pressure, T is the temperature, E is the total energy, μ is the molecular viscosity, κ is the thermal conductivity, and C_v is the specific heat at constant volume. C_v is assumed to be constant. The above equations are supplemented by the ideal gas law, $p = \rho R T$, and the viscosity power law, $\mu/\mu_r = (T/T_r)^{0.76}$ [29]. Here, R is the ideal gas constant, μ_r and T_r are reference viscosity and temperature, respectively. The Prandtl number $Pr \equiv C_p\mu/\kappa$ is set to 0.7 and $\gamma \equiv C_p/C_v$ to 1.4; C_p is the specific heat at constant pressure.

The equations above can be combined to give the internal energy and entropy equations:

$$\frac{\partial \rho e}{\partial t} + \frac{\partial \rho e u_j}{\partial x_j} + p\frac{\partial u_j}{\partial x_j} = \tau_{ij}\frac{\partial u_i}{\partial x_j} + \frac{\partial}{\partial x_j}\left(\kappa \frac{\partial T}{\partial x_j}\right),$$ (5)

$$\frac{\partial \rho s}{\partial t} + \frac{\partial \rho s u_j}{\partial x_j} = \frac{1}{T}\left[\tau_{ij}\frac{\partial u_i}{\partial x_j} + \frac{\partial}{\partial x_j}\left(\kappa \frac{\partial T}{\partial x_j}\right)\right],$$ (6)

$$= \frac{\partial}{\partial x_j}\left(\frac{\kappa}{T}\frac{\partial T}{\partial x_j}\right) + \frac{\tau_{ij}}{T}\frac{\partial u_i}{\partial x_j} + \frac{\kappa}{T^2}\frac{\partial T}{\partial x_j}\frac{\partial T}{\partial x_j}.$$ (7)

Here, the internal energy per unit mass e is given by $e = C_v T$ and the entropy s by

$$s = C_v \ln(p\rho^{-\gamma}).$$ (8)

Multiplying (6) by $2s$ and (1) by s^2, one obtains upon adding

$$\frac{\partial \rho s^2}{\partial t} + \frac{\partial \rho s^2 u_j}{\partial x_j} = \frac{2s}{T}\left[\tau_{ij}\frac{\partial u_i}{\partial x_j} + \frac{\partial}{\partial x_j}\left(\kappa \frac{\partial T}{\partial x_j}\right)\right].$$ (9)

The convective terms in (6) and (9) are in divergence form, which implies that their contribution to the volume averages $\overline{\rho s}$ and $\overline{\rho s^2}$ results in boundary terms. Also, the last two terms in (7) are easily shown to be positive, which means that $\overline{\rho s}$ should not decrease in time in a periodic domain.

2.2. Convective terms of the entropy equation

Applying a high order central scheme to the conservative form of the Navier–Stokes equations as written in (1)–(3) can lead to numerical instabilities in DNS or LES of compressible isotropic turbulence [17,20,30,31]. As mentioned in Section 1, these instabilities are lessened by preventing the convective term of the momentum equation from artificially producing or dissipating global kinetic energy [17]. Looking at $\overline{\rho s}$ in these unstable simulations, one would find that it decreases with time, which is a clear violation of the second law of thermodynamics. This non-physical entropy loss can be traced to the convective terms. Moreover, it is found that the contribution of these terms to $\overline{\rho s^2}$ is not zero as discussed in the last section. We propose that forcing the nonlinear terms not to spuriously contribute to $\overline{\rho s}$ and $\overline{\rho s^2}$ will greatly enhance the nonlinear stability properties of a numerical scheme. It is in this sense the phrase "entropy conservation" is used in this paper. The improvement is demonstrated for compressible isotropic turbulence simulations in the numerical experiments of the next section.

Assuming no time stepping errors, one approach to achieve the requirements above is to use the entropy equation (6) instead of the internal or total energy equations. Furthermore, the erroneous contribution to $\overline{\rho s^2}$ is nullified by writing the convective term in (6) in a skew-symmetric form as done by Feiereisen et al. [17] for the momentum equation and by Blaisdell et al. [32] for both momentum and scalar equations:

$$\frac{\partial \rho a u_j}{\partial x_j} \to \frac{1}{2} \frac{\partial \rho a u_j}{\partial x_j} + \frac{a}{2} \frac{\partial \rho u_j}{\partial x_j} + \frac{\rho u_j}{2} \frac{\partial a}{\partial x_j}. \tag{10}$$

With $a = s$, (10) gives the modified form of the convective term in (6), which then becomes

$$\frac{\partial \rho s}{\partial t} + \frac{1}{2} \frac{\partial \rho s u_j}{\partial x_j} + \frac{s}{2} \frac{\partial \rho u_j}{\partial x_j} + \frac{\rho u_j}{2} \frac{\partial s}{\partial x_j} = \frac{1}{T} \left[\tau_{ij} \frac{\partial u_i}{\partial x_j} + \frac{\partial}{\partial x_j} \left(\kappa \frac{\partial T}{\partial x_j} \right) \right]. \tag{11}$$

The contribution of the convective terms in (11) to both $\overline{\rho s}$ and $\overline{\rho s^2}$ can easily be verified to sum up to boundary terms. Summing (11) over the volume and assuming summation by parts holds for the spatial derivative operator (see below), the convective terms reduce to

$$\sum_{j,\ \text{outflow}} \rho s u_j - \sum_{j,\ \text{inflow}} \rho s u_j. \tag{12}$$

To obtain the effect on $\overline{\rho s^2}$, one has to multiply (11) by $2s$, use (1), and then sum over the volume. This also yields boundary terms

$$\sum_{j,\ \text{outflow}} \rho s^2 u_j - \sum_{j,\ \text{inflow}} \rho s^2 u_j. \tag{13}$$

Therefore, given a numerical solution that satisfies (11), $\overline{\rho s}$ and $\overline{\rho s^2}$ are guaranteed not to be spuriously affected by the convective terms, assuming no time stepping errors. We note here that this is the approach used by [17] to show that $\overline{\rho u_i}$ and $\overline{\rho \frac{u_i u_i}{2}}$ are not affected by the nonlinear term in the momentum equation in a periodic domain. The procedure outlined above is easily carried when the variables are arranged on a regular grid. The implementation on a staggered grid is outlined in [31].

For periodic domains, the summation by parts property takes the form

$$\sum_{j=1}^{N} u_j \frac{\mathrm{d} v_j}{\mathrm{d} x} = - \sum_{j=1}^{N} v_j \frac{\mathrm{d} u_j}{\mathrm{d} x}, \tag{14}$$

and was shown to hold for central schemes by Mansour et al. [12]. We highlight the proof in Section 3.2. For non-periodic boundary conditions, Strand [33] showed it is possible to construct finite difference operators (central inside the domain and non-central near the boundaries) such that

$$\sum_{j=1}^{N} h_j u_j \frac{\mathrm{d}v_j}{\mathrm{d}x} = u_j v_j |_{j=1}^{N} - \sum_{j=1}^{N} h_j v_j \frac{\mathrm{d}u_j}{\mathrm{d}x} \tag{15}$$

is satisfied. Here h_j are the weights of the inner product and are positive numbers. These weights have to be used when summing over the domain in order to obtain (12) and (13).

2.3. Equivalent energy equations

An equivalent approach is to use the internal or total energy equations and modify their nonlinear terms so that a proper combination of the working equations yields (11). This can be done as follows. Substituting for s from (8) in (11) and ignoring the viscous terms, we get

$$\frac{C_v \rho}{p} \frac{\partial p}{\partial t} + (s - \gamma C_v) \frac{\partial \rho}{\partial t} + \frac{1}{2} \frac{\partial \rho s u_j}{\partial x_j} + \frac{s}{2} \frac{\partial \rho u_j}{\partial x_j} + \frac{\rho u_j}{2} \frac{\partial s}{\partial x_j} = 0. \tag{16}$$

Substituting for $\partial \rho / \partial t$ from (1)

$$\frac{\partial p}{\partial t} + \frac{p}{\rho} \left(\gamma - \frac{s}{2C_v} \right) \frac{\partial \rho u_j}{\partial x_j} + \frac{p}{2C_v \rho} \frac{\partial \rho u_j s}{\partial x_j} + \frac{p u_j}{2C_v} \frac{\partial s}{\partial x_j} = 0. \tag{17}$$

Adding the viscous terms and using $p = (\gamma - 1)\rho e$, we obtain another form of (5)

$$\frac{\partial \rho e}{\partial t} + e \left(\gamma - \frac{s}{2C_v} \right) \frac{\partial \rho u_j}{\partial x_j} + \frac{e}{2C_v} \frac{\partial \rho s u_j}{\partial x_j} + \frac{\rho e u_j}{2C_v} \frac{\partial s}{\partial x_j} = \tau_{ij} \frac{\partial u_i}{\partial x_j} + \frac{\partial}{\partial x_j} \left(\kappa \frac{\partial T}{\partial x_j} \right). \tag{18}$$

It can be easily verified that (11) is the result of multiplying (18) by $(\gamma - 1)C_v \rho p^{-1}$ and adding to (1) multiplied by $(s - \gamma C_v)$. The following equation can be similarly derived for the total energy:

$$\frac{\partial E}{\partial t} + e \left(\gamma - \frac{s}{2C_v} \right) \frac{\partial \rho u_j}{\partial x_j} + \frac{e}{2C_v} \frac{\partial \rho s u_j}{\partial x_j} + \frac{\rho e u_j}{2C_v} \frac{\partial s}{\partial x_j} + u_j \frac{\partial p}{\partial x_j} + \frac{u_i}{2} \frac{\partial \rho u_i u_j}{\partial x_j} + \frac{\rho u_j u_i}{2} \frac{\partial u_i}{\partial x_j}$$
$$= \tau_{ij} \frac{\partial u_i}{\partial x_j} + u_i \frac{\partial \tau_{ij}}{\partial x_j} + \frac{\partial}{\partial x_j} \left(\kappa \frac{\partial T}{\partial x_j} \right). \tag{19}$$

Eqs. (11), (18), and (19) share the same nonlinear numerical stability properties. Also, these equations are equivalent numerically for DNS and "no-model" calculations as long as time stepping errors are negligible. For LES calculations, differences might arise depending on how the subgrid-scale model is implemented. For problems involving shocks with fixed mean position, (19) might be useful if incorporated in a suitable shock capturing scheme.

2.4. Skew-symmetric form

As mentioned earlier, the skew-symmetric form in (10) was discussed in the context of conservation by Feiereisen et al. [17] and Blaisdell et al. [32]. However, this form was used differently by Blaisdell et al. [22] and Spyropoulos and Blaisdell [30]. In these studies, the convective terms in (2) and (5) were discretized according to

$$\frac{\partial \rho a u_j}{\partial x_j} \rightarrow \frac{1}{2}\frac{\partial \rho a u_j}{\partial x_j} + \frac{\rho a}{2}\frac{\partial u_j}{\partial x_j} + \frac{u_j}{2}\frac{\partial \rho a}{\partial x_j} \tag{20}$$

with $a = u_i$ for (2) and $a = e$ for (5). The forms in (10) and (20) are not equivalent numerically in general. For one thing, the boundary terms (13) do not follow if (20) is used, even if the convective term in (1) is split. The reason for using this different splitting might have been that the aim in [22] was to minimize aliasing errors and not to enforce conservation. It was found in [22] that the error in calculating the spectral derivative of a product gh is reduced by using the form

$$\frac{\partial gh}{\partial x} \rightarrow \frac{1}{2}\frac{\partial gh}{\partial x} + \frac{g}{2}\frac{\partial h}{\partial x} + \frac{h}{2}\frac{\partial g}{\partial x}. \tag{21}$$

From this point of view, it does not matter how the derivative of a triple product is written, as long as it is split according to (21). Setting $g = \rho a$ and $h = u_j$ in (21) yields (20). Also, it is easier to calculate $(\rho e u_j)_{,j}$ in a spectral code using (20) since ρe, and not e, is the variable being advanced in time. This splitting was adopted for finite difference schemes by Ducros et al. [4]. Although the form (20) behaves better than the divergence [1] and non-conservative [2] forms [22], it is less robust than (10), as seen in the next section.

Although there is no formal reason to use (10) in (5), it can be justified in the light of (11). The good performance of this approach will be confirmed through numerical simulations below. We note that re-casting the nonlinear terms of the total energy equation in the form (10) will not be successful [31]. The proper method to derive a total energy equation that inherits the same stability properties of the internal energy equation is by multiplying the modified form of (2) by u_i and adding to the modified form of (5). By modified forms of (2) and (5) we mean the convective terms are discretized using (10). The resulting total energy equation is

$$\frac{\partial E}{\partial t} + \frac{u_i}{2}\frac{\partial \rho u_i u_j}{\partial x_j} + \frac{\rho u_j u_i}{2}\frac{\partial u_i}{\partial x_j} + \frac{1}{2}\frac{\partial \rho e u_j}{\partial x_j} + \frac{e}{2}\frac{\partial \rho u_j}{\partial x_j} + \frac{\rho u_j}{2}\frac{\partial e}{\partial x_j} + p\frac{\partial u_j}{\partial x_j} + u_j\frac{\partial p}{\partial x_j}$$

$$= \tau_{ij}\frac{\partial u_i}{\partial x_j} + u_i\frac{\partial \tau_{ij}}{\partial x_j} + \frac{\partial}{\partial x_j}\left(\kappa\frac{\partial T}{\partial x_j}\right). \tag{22}$$

Comparing to (3), we infer that the nonlinear terms in (22) are the result of applying the non-conservative form to $[(\rho u_i u_j)u_i]_{,j}$ and $(p u_j)_{,j}$ and the skew-symmetric form (10) to $(\rho e u_j)_{,j}$. The difference in robustness between internal and total energy formulations reported in [3,23] is reconciled with the procedure just outlined.

3. Numerical simulations

In this section, we use compressible isotropic turbulence simulations to compare the numerical stability of the formulations discussed in the previous section to the methods cited in Section 1.

3.1. Numerical methods

The different methods are labeled below, with method A representing the new formulation discussed in the previous section.

---

[1] Simply $(gh)'$.

[2] $(gh)' \rightarrow g'h + gh'$.

Method A: Eqs. (1), (2), and (18) are solved, with the form (10) implemented in (2). This method conserves ρ locally and ρu_i globally in the limit of zero viscosity. In addition, $\overline{\rho \frac{u_i u_i}{2}}$, $\overline{\rho s}$, and $\overline{\rho s^2}$ are not spuriously affected by the nonlinear terms.

Method B: Entropy splitting technique in [1,2]. This method only conserves $\rho e^{s/\beta(1-\gamma)}$ globally in the limit of zero viscosity. β was set to 2 as values around 2 were found to give the best results for most of the simulations considered in this work.

Method C: Eqs. (1), (2), and (5) are solved with the convective terms discretized as in (10). This method conserves ρ locally, ρu_i and E globally in the limit of zero viscosity. In addition, $\overline{\rho \frac{u_i u_i}{2}}$ is not spuriously affected by the nonlinear terms.

Method D: Staggered method used by [3]. This method is attractive because it locally conserves ρ, ρu_i, and E while providing additional robustness compared to a collocated scheme using non-conservative splitting of the nonlinear terms.

Method E: Eqs. (1)–(3) are solved. The convective terms in (2) are written according to (20) and those in (3) according to (21). This scheme is similar to the skew-symmetric-like schemes suggested by Ducros et al. [4]. Method E conserves ρ locally, ρu_i and E globally in the limit of zero viscosity.

The third order Runge–Kutta time stepping scheme is used along with the sixth order compact finite difference scheme [34]:

$$\alpha u'_{j-1} + u'_j + \alpha u'_{j+1} = a \frac{u_{j+1} - u_{j-1}}{2\Delta} + b \frac{u_{j+2} - u_{j-2}}{4\Delta}, \tag{23}$$

where $\alpha = 1/3$, $a = 14/9$, $b = 1/9$, and Δ the grid size. The test cases performed are similar to those performed in [3,18,20,30]. The initial energy spectrum is given by

$$E_s(k) = \frac{16}{3} \sqrt{\frac{2}{\pi}} M_{t_0}^2 \frac{k^4}{k_0^5} e^{-2k^2/k_0^2}, \tag{24}$$

where M_{t_0} is the turbulence Mach number and k_0 is the most energetic scale in the initial field. The eddy turnover time for this spectrum is $\tau = 2\sqrt{3}/(k_0 M_{t_0})$. The initial density and temperature fields are uniformly set to ρ_0 and T_0. The dynamic model is implemented according to [18,35]. The filter is the explicit seven point least-squares filter derived in [30] and used by [3].

3.2. Summation by parts for central schemes

For explicit central schemes, e.g. the fourth order scheme

$$u'_j = \frac{-u_{j+2} + 8u_{j+1} - 8u_{j-1} + u_{j-2}}{12\Delta}, \tag{25}$$

it is easy to show that the formula (14) holds by simply substituting for u'_j and v'_j from (25) and using the periodicity condition. For implicit schemes, e.g. (23), the proof is carried as in [12,15] by using the Fourier transform representation of u_j and v_j. With

$$u_j = \sum_{n=-N/2+1}^{N/2} \hat{u}_n e^{i2\pi jn/N}, \tag{26}$$

(23) yields the following formula for u'_j:

$$u'_j = \sum_{n=-N/2+1}^{N/2} ik' \hat{u}_n e^{i2\pi jn/N}. \tag{27}$$

In the last two equations, $\hat{u}_n$ is the discrete Fourier transform of u_j, i is the imaginary unit number, N is the number of grid points in one direction, and k' is the modified wavenumber of the difference scheme given by

$$k' = \frac{a\sin(2\pi n/N) + b/2\sin(4\pi n/N)}{(2\pi/N)[1 + 2\alpha\cos(2\pi n/N)]}.$$

With some algebraic manipulations, (26), (27), and similar expressions for v_j and v'_j can be shown to satisfy (14).

3.3. Validation

We first validate method A by performing DNS of compressible isotropic turbulence on a 64^3 grid with $Re_\lambda = 30$, $M_{t_0} = 0.3$, and $k_0 = 4$. Similar parameters have been used in many studies, [21] among others, and are deemed adequate for DNS. Comparisons are made against a spectral simulation conducted using a specific volume formulation instead of a density formulation. As suggested by Lee et al. [36], this procedure avoids the division operator and allows full de-aliasing. The evolution of the non-dimensional turbulent kinetic energy and thermodynamic fluctuations versus time is shown in Fig. 1. The various non-dimensional quantities are defined by: $k' = (u_{1,\text{rms}}^2 + u_{2,\text{rms}}^2 + u_{3,\text{rms}}^2)/(c_0^2 M_{t_0}^2)$, $p' = p_{\text{rms}}/(\gamma p_0 M_{t_0}^2)$, $T' = T_{\text{rms}}/[(\gamma-1)T_0 M_{t_0}^2]$, and $v' = v_{\text{rms}}/(v_0 M_{t_0}^2)$. Here v is the specific volume, $v = 1/\rho$, and c_0 is the speed of sound. The plots reveal a very good agreement between the two methods for all statistics, and this validates method A. We note here that increasing the grid to 128^3 for method A would basically yield the same results.
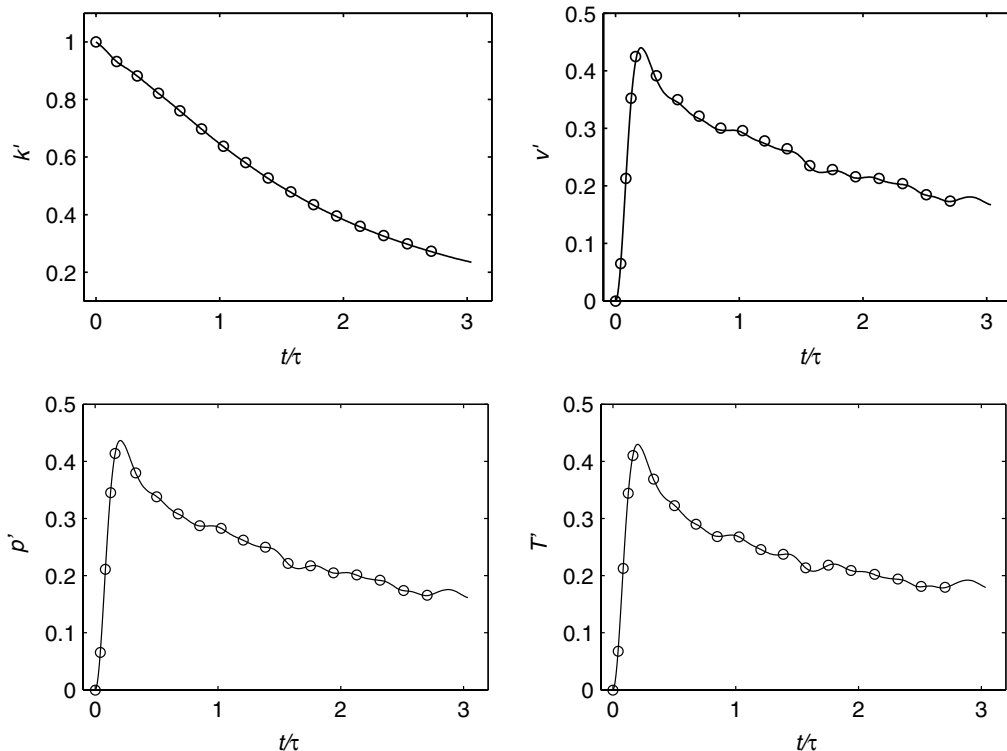

Fig. 1. 64^3 DNS, $M_{t_0} = 0.3$, $k_0 = 4$, $Re_\lambda = 30$, —: method A, ◯: de-aliased spectral.

3.4. Unresolved simulations results

In order to test the nonlinear numerical stability of the different methods, we carry coarse grid isotropic turbulence simulations at increasingly high Reynolds numbers, without any model. These kind of tests provided to be useful for incompressible simulations, where stable schemes force the kinetic energy to decay for finite Reynolds number and remain constant in the limit of zero viscosity. This behavior is predicted by the incompressible equations, but not the compressible ones. Kraichnan [37], however, showed that there is
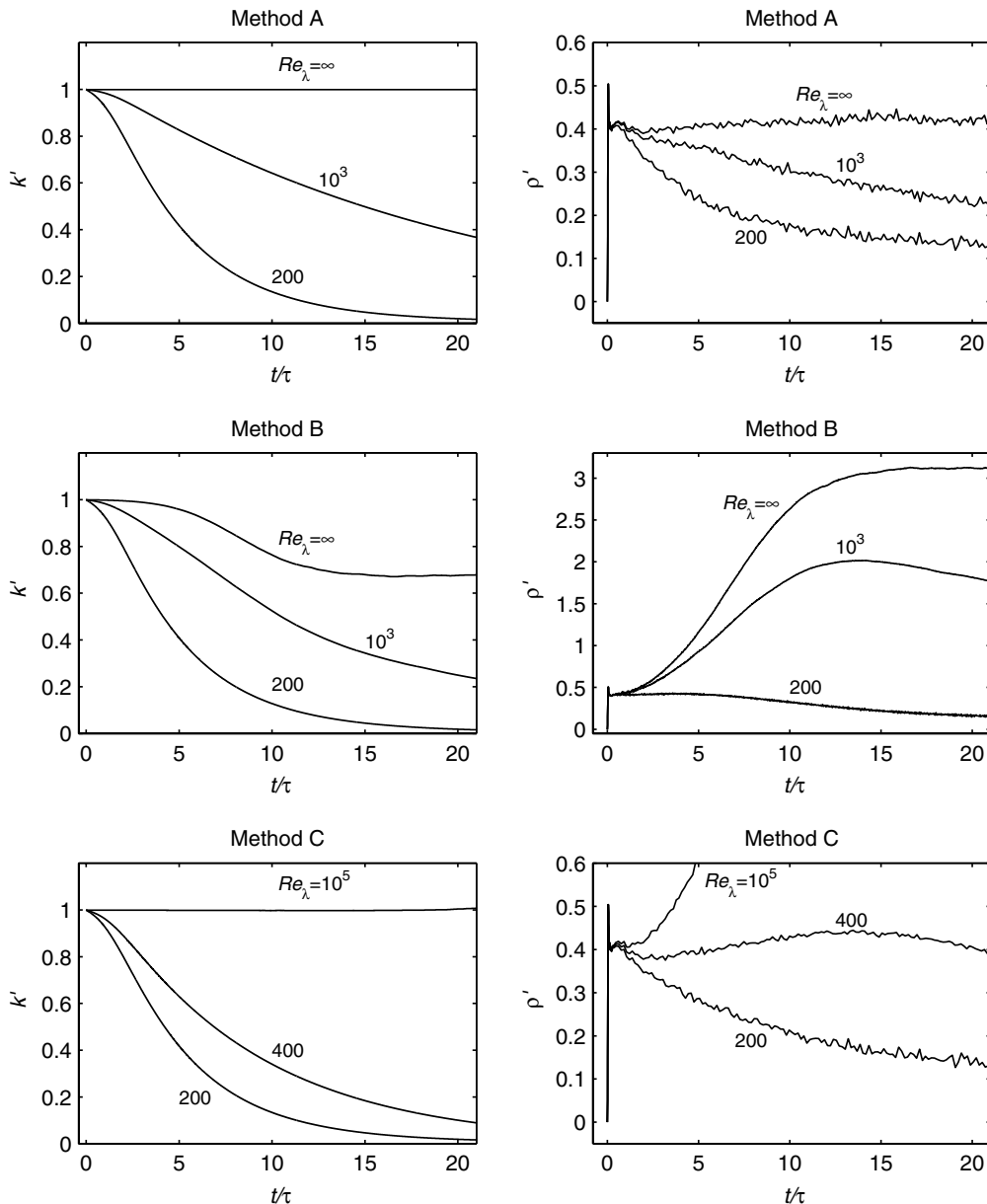
Fig. 2. $M_{t_0} = 0.07$, $k_0 = 6$, Methods A, B, and C.

an equipartition between the different energy modes of the truncated isothermal Euler equations at low Mach number. For this purpose, we performed a fully de-aliased spectral simulation of the full Euler equations on a 32^3 grid with $M_{t_0} = 0.07$ and $k_0 = 6$ and ran it for a time of 20τ. After a short transient, the kinetic energy and thermodynamic fluctuations were found to decay for finite Re_λ and remain approxi-
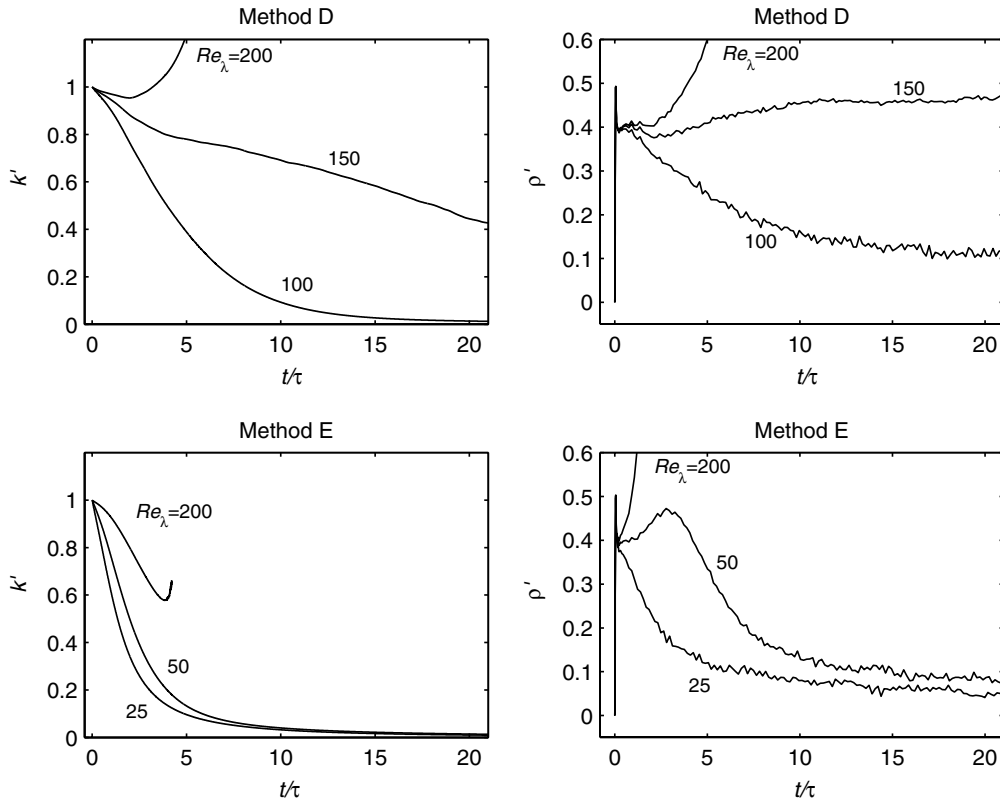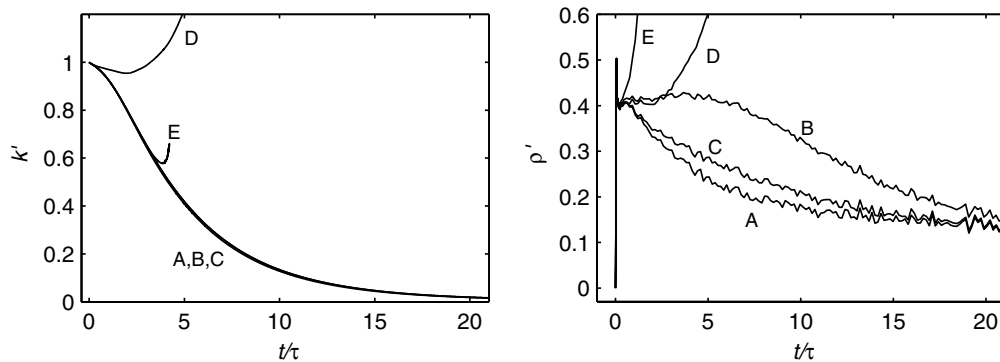

Fig. 3. $M_{t_0} = 0.07$, $k_0 = 6$, Methods D and E.

Fig. 4. $M_{t_0} = 0.07$, $k_0 = 6$, $Re_\lambda = 200$.

mately constant for very high Re_λ. The constant values were $k' \approx 1$ and $v' \approx p' \approx T' \approx 0.35$. Moreover, it was found that shocklets (regions where local $M_t \geqslant 1$) did not develop in these calculations. In fact, the local Mach number was always below 0.2. Also, the spectral simulations would blow up for high Re_λ if de-aliasing was not performed. Below, we use the simulations discussed here to investigate nonlinear numerical stability properties of methods A, B, C, D, and E. We note that results from coarse grid simulations at high
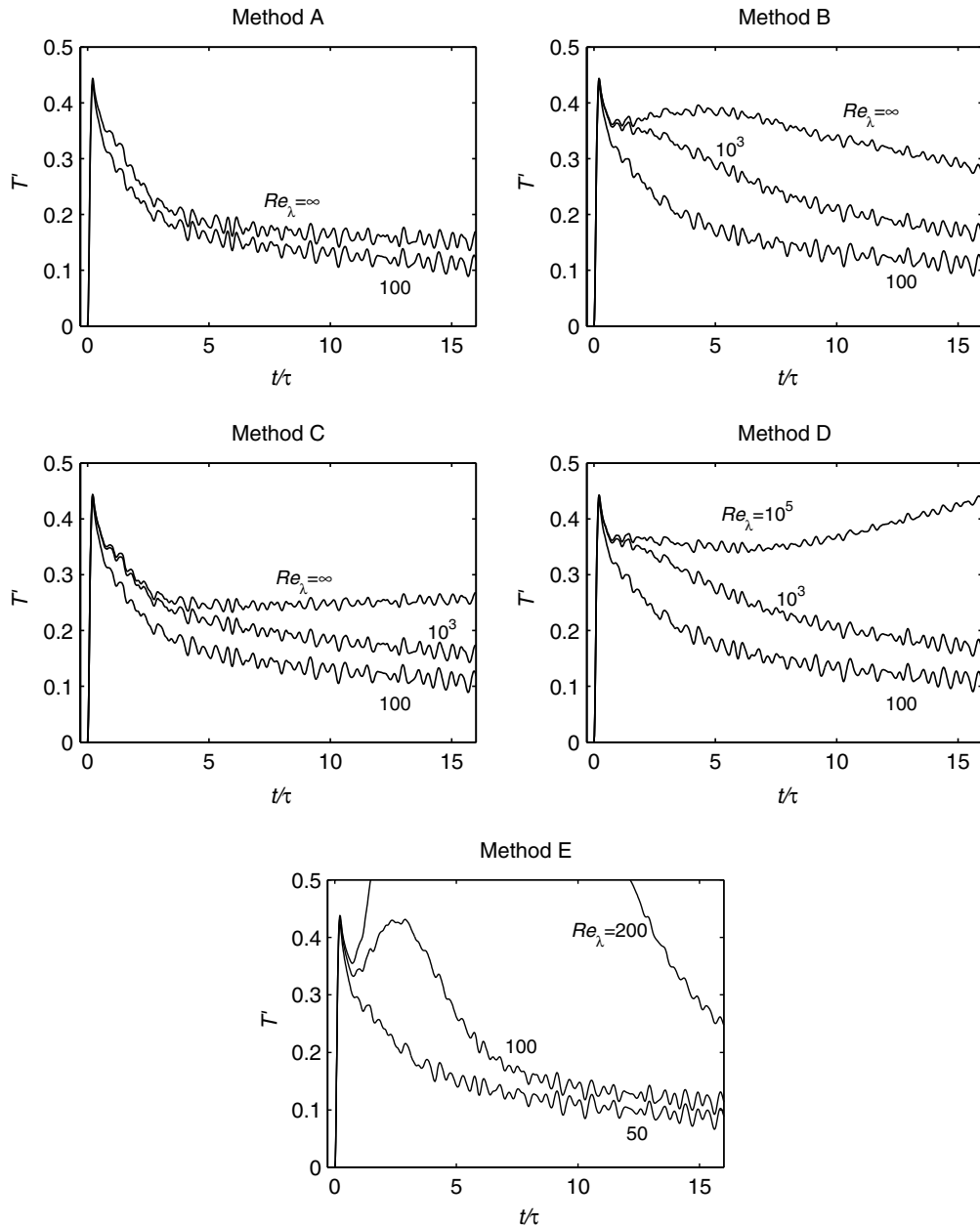

Fig. 5. $M_{t_0} = 0.3$, $k_0 = 4$, LES.

Reynolds number do not describe turbulence physics; a subgrid scale model has to be incorporated for this purpose. However, these simulations provide a test for nonlinear numerical stability and the behavior of the inviscid truncated equations can be predicted by means of statistical mechanics [38–40].

The non-dimensional turbulent kinetic energy k' and density fluctuation $\rho' = \rho_{rms}/(\rho_0 M_{t_0}^2)$ are shown in Figs. 2 and 3 for several values of the Reynolds number. For method A, fluctuations decay at finite Re_λ and reach an equilibrium at infinite Re_λ, in good agreement with the spectral results mentioned above. For method B, kinetic energy always decays while density fluctuations greatly amplify for high Reynolds number. An equilibrium is also attained at infinite Re_λ. The behavior and equilibrium values of method B do not compare well with those of the de-aliased spectral method. In method B, there is a significant transfer of energy from vorticity modes to entropy modes [41,42], that is from kinetic energy to density fluctuations. This could be attributed to the lack of conservation properties in method B, which leads to wrong channeling of energy. Also, it is found that high Re_λ simulations would blow up if β is changed to 1.8 or 2.2. Methods C, D, and E yield negative density values for Re_λ greater than 500, 150, and 100, respectively. The instabilities lead to kinetic energy increase in D but not in C or E. The five methods are differentiated in Fig. 4, where results are plotted for $Re_\lambda = 200$. For this Reynolds number, methods D and E are unstable. Methods A, B, and C give identical results for the kinetic energy but not for the density fluctuations: ρ' in method B suffers from instabilities, which are less apparent in method C and absent in method A. Note that method C does not perform well at high Re_λ. Similar trend in the results was obtained for a 16^3 grid.

For higher initial turbulent Mach number, shocks might eventually develop after several eddy turnover times depending on the Reynolds number. Because of the low resolution and the absence of any shock capturing scheme in the current simulations, instabilities build up and fluctuations diverge from the equilibrium values. At infinite Re_λ, this occurs when M_{t_0} is around 0.2 for the spectral method and 0.09 for method A with the sixth order compact scheme. For non-compact spatial schemes, the critical initial Mach number will be lower for the same 32^3 grid: M_{t_0} is 0.07 and 0.05 for the fourth and second order schemes, respectively. Also, the equilibrium values become less accurate for low order schemes. This behavior is due to large truncation errors in these methods. The high order compact scheme used with the current entropy conserving formulation represents the closest match to the de-aliased spectral method.

3.5. LES results

We next show LES results for $M_{t_0} = 0.3$ and $k_0 = 4$. A spectral simulation with these parameters (with the dynamic model computed in the physical space) would result in k', T', v', and p' decaying at all Re_λ after
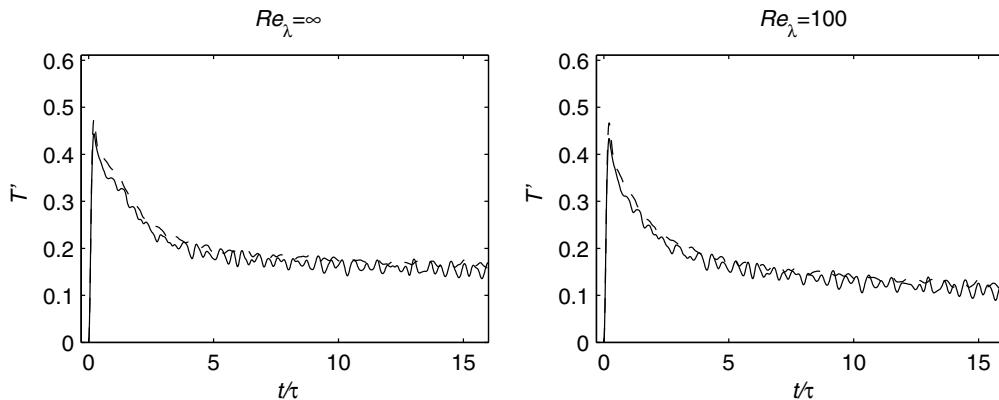

Fig. 6. Mesh refinement for method A, $M_{t_0} = 0.3$, $k_0 = 4$, —: 32^3, ––: 64^3.

a short initial transient. A stable finite difference scheme is therefore expected to yield a similar decay. The non-dimensional temperature fluctuations T' are plotted for several values of the Reynolds number in Fig. 5. After a small time, T' reaches a peak approximately equal to the equilibrium value of the previous simulations. For method A, T' decays after the peak at all Re_λ. This is not the case for method B, where for $Re_\lambda > 10^3$, T' reaches another peak before it finally decays. As in the previous case, method C gives very satisfactory results. T' decays as in A as long as $Re_\lambda < 10^5$. For infinite Reynolds number, instabilities start
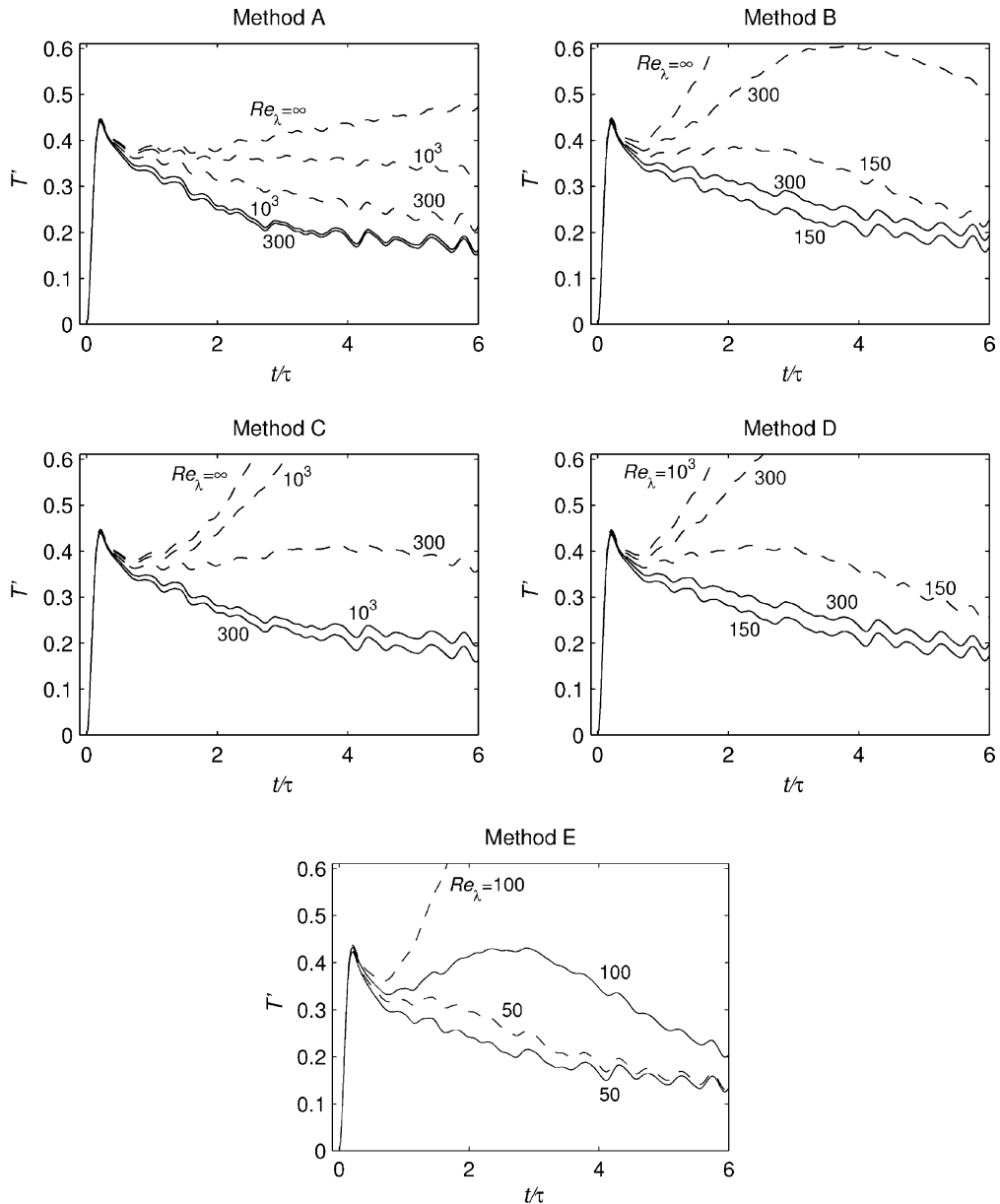
Fig. 7. $M_{t_0} = 0.3$, $k_0 = 4$, —: model turned on, −−: model turned off.

building up but very slowly. Method D become unstable for $Re_\lambda > 2000 : T'$ gradually increases until a negative density is obtained. Instabilities appear in method E at low Re_λ and grow at a very fast rate. A grid refinement study with a 64^3 grid was done for method A . Results for the 32^3 and 64^3 grids are shown in Fig. 6 and they compare very well.

In order to quantify the subgrid scale effects in these simulations, we show in Fig. 7 results with the dynamic model switched off. In this case, the decay rates in T' are much slower and instabilities occur at lower Reynolds number. For $M_{t_0} = 0.3$, method A is no longer stable at infinite Re_λ, as discussed above. Methods A, B, and C become unstable without the model for $Re_\lambda > 10^4$ while methods D and E for Re_λ greater than 300 and 100. The growth of instabilities for method A is the least dramatic of all methods. The difference between model and ''no-model'' results shows the significance of the subgrid scale dissipation. However, the presence of subgrid scale model is not always sufficient to remove nonlinear instabilities. A scheme with good conservation properties is necessary for simulations with low molecular and subgrid scale dissipation.

4. Conclusion

We were able to use a high order compact central finite difference scheme to simulate compressible turbulent fluctuations at very high Reynolds numbers without artificial dissipation or filtering. This was accomplished by preventing the nonlinear terms from spuriously contributing to $\overline{\rho s}$ and $\overline{\rho s^2}$ through proper implementation of the skew-symmetric form. Several other schemes were shown to be inadequate at large Reynolds numbers. We also showed that using the skew-symmetric splitting for the purpose of reducing aliasing errors in finite difference calculations is not always useful. Application of the methodologies discussed above to simulations involving shocks requires further investigation.

Acknowledgements

References

[1] H.C. Yee, M. Vinokur, M.J. Djomehri, Entropy splitting and numerical dissipation, J. Comput. Phys. 162 (2000) 33–81.
[2] N.D. Sandham, Q. Li, H.C. Yee, Entropy splitting for high-order numerical simulation of compressible turbulence, J. Comput. Phys. 178 (2002) 307–322.
[3] S. Nagarajan, S.K. Lele, J.H. Ferziger, A robust high-order compact method for large eddy simulation, J. Comput. Phys. 191 (2) (2003) 392–419.
[4] F. Ducros, F. Laporte, T. Souleres, V. Guinot, P. Moinat, B. Caruelle, High-order fluxes for conservative skew-symmetric-like schemes in structured meshes, J. Comput. Phys. 161 (2000) 114–139.
[5] N.A. Phillips, An example of non-linear computational instability, in: The Atmosphere and the Sea in Motion, Rockefeller Institute Press and the Oxford University Press, New York, 1959, pp. 501–504.
[6] D.K. Lilly, On the computational stability of numerical solutions of time-dependent non-linear geophysical fluids dynamics problems, Mon. Weather Rev. 93 (1965) 11–26.
[7] S. Ghosal, An analysis of numerical errors in large-eddy simulations of turbulence, J. Comput. Phys. 125 (1) (1996) 187–206.
[8] Y. Morinishi, T.S. Lund, O.V. Vasilyev, P. Moin, Fully conservative higher order finite difference schemes for incompressible flow, J. Comput. Phys. 143 (1) (1998) 90–124.

 [9] P. Moin, Fundamentals of Engineering Numerical Analysis, Cambridge University Press, Cambridge, 2001.
[10] T.A. Zang, On the rotation and skew-symmetric forms for incompressible flow simulations, Appl. Numer. Math. 7 (1) (1991) 27–40.
[11] K. Horiuti, Comparison of conservative and rotational forms in large eddy simulation of turbulent channel flow, J. Comput. Phys. 71 (2) (1987) 343–370.
[12] N.N. Mansour, P. Moin, W.C. Reynolds, J.H. Ferziger, Improved methods for large eddy simulations of turbulence, Turbulent Shear Flows 1 (1979) 386–401.
[13] F.H. Harlow, J.E. Welch, Numerical calculation of time-dependent viscous incompressible flow of fluids with free surface, Phys. Fluids 8 (1965) 2182–2189.
[14] J. Kim, P. Moin, Application of a fractional-step method to incompressible Navier–Stokes equations, J. Comput. Phys. 59 (2) (1985) 308–323.
[15] A.G. Kravchenko, P. Moin, On the effect of numerical errors in large eddy simulations of turbulent flows, J. Comput. Phys. 131 (2) (1997) 310–322.
[16] C.D. Pierce, P. Moin, Progress-variable approach for large eddy simulation, Report TF-80, Flow Phys. Comput. Div., Mech. Eng., Stanford University, 2001.
[17] W.J. Feiereisen, W.C. Reynolds, J.H. Ferziger, Numerical simulation of a compressible, homogeneous, turbulent shear flow, Report TF-13, Thermosci. Div., Mech. Eng., Stanford University, 1981.
[18] P. Moin, K. Squires, W. Cabot, S. Lee, A dynamic subgrid-scale model for compressible turbulence and scalar transport, Phys. Fluids A 3–11 (1991) 2746–2757.
[19] T. Dubois, J.A. Domaradzki, A. Honein, The subgrid-scale estimation model applied to large eddy simulations of compressible turbulence, Phys. Fluids 14 (2002) 1781–1801.
[20] R. Samtaney, D.I. Pullin, B. Kosovic, Direct numerical simulation of decaying compressible turbulence and shocklet statistics, Phys. Fluids 13 (5) (2001) 1415–1430.
[21] S. Lee, S.K. Lele, P. Moin, Simulation of spatially evolving turbulence and the applicability of Taylor's hypothesis in compressible flow, Phys. Fluids A 4 (7) (1992) 1521–1530.
[22] G.A. Blaisdell, E.T. Spyropoulos, J.H. Qin, The effect of the formulation of non-linear terms on aliasing errors in spectral methods, Appl. Numer. Math. 21 (3) (1996) 207–219.
[23] S. Lee, Large eddy simulation of shock–turbulence interaction, Annual Research Briefs, Center for Turbulence Research, 1991, pp. 73–84.
[24] A. Harten, On the symmetric form of systems of conservation laws, J. Comput. Phys. 49 (1983) 151–164.
[25] E. Tadmor, Skew selfadjoint form for systems of conservation laws, J. Math. Anal. Appl. 103 (1984) 428–442.
[26] P. Olsson, J. Oliger, Energy and maximum norm estimates for non linear conservation laws, RIACS Technical Report 94-01, NASA Ames Research Center, 1994.
[27] M. Gerritsen, Designing an efficient solution strategy for fluid flows, Ph.D. Thesis, Stanford University, 1996.
[28] M. Gerritsen, P. Olsson, Designing an efficient solution strategy for fluid flows. I. A stable high order finite difference scheme and sharp shock resolution for the Euler equations, J. Comput. Phys. 129 (1996) 245–262.
[29] E.R. Van Driest, Investigation of laminar boundary layer in compressible fluids using the Crocco method, NACA TN 2597, 1952.
[30] E.T. Spyropoulos, G.A. Blaisdell, Evaluation of the dynamic model for simulations of compressible decaying isotropic turbulence, AIAA J. 7 (5) (1996) 27–40.
[31] A.E. Honein, Numerical aspects of compressible turbulence simulations, Ph.D. Thesis, Stanford University, 2004.
[32] G.A. Blaisdell, N.N. Mansour, W.C. Reynolds, Numerical simulations of compressible homogeneous turbulence, Report TF-50, Thermosci. Div., Mech. Eng., Stanford University, 1991.
[33] B. Strand, Summation by parts for finite difference approximations for d/dx, J. Comput. Phys. 110 (1994) 47–67.
[34] S.K. Lele, Compact finite difference schemes with spectral-like resolution, J. Comput. Phys. 103 (1992) 16.
[35] D.K. Lilly, A proposed modification of the Germano subgrid-scale closure method, Phys. Fluids A 4 (3) (1992) 633–635.
[36] S. Lee, P. Moin, S.K. Lele, Interaction of isotropic turbulence with a shock wave, Report TF-52, Thermosci. Div., Mech. Eng., Stanford University, 1992.
[37] R.H. Kraichnan, On the statistical mechanics of an adiabatically compressible fluid, J. Acoust. Soc. Am. 27 (3) (1955) 438–441.
[38] L. Onsager, Statistical hydrodynamics, Nuovo Cimento Suppl. 6 (1949) 279–286.
[39] R.H. Kraichnan, Inertial ranges in two-dimensional turbulence, Phys. Fluids 10 (1967) 1417–1423.
[40] C. Basdevant, R. Sadourny, Ergodic properties of inviscid truncated models of two-dimensional incompressible flows, J. Fluid Mech. 69 (1975) 673–688.
[41] L.S.G. Kovasznay, Turbulence in supersonic flow, J. Aeronaut. Sci. 20 (1953) 657–674.
[42] B.T. Chu, L.S.G. Kovasznay, Nonlinear interactions in a viscous heat-conducting compressible gas, J. Fluid Mech. 3 (1958) 494–514.